Chromosome looping in yeast: telomere pairing and coordinated movement reflect anchoring efficiency and territorial organization

Kerstin Bystricky,[1] Thierry Laroche,[1] Griet van Houwe,[1] Marek Blaszczyk,[2] and Susan M. Gasser[1]

[1]Department of Molecular Biology and NCCR Frontiers in Genetics, University of Geneva, 1211 Geneva 4, Switzerland
[2]Institute of Applied Mathematics, University of Lausanne, 1015 Lausanne, Switzerland

Long-range chromosome organization is known to influence nuclear function. Budding yeast centromeres cluster near the spindle pole body, whereas telomeres are grouped in five to eight perinuclear foci. Using live microscopy, we examine the relative positions of right and left telomeres of several yeast chromosomes. Integrated lac and tet operator arrays are visualized by their respective repressor fused to CFP and YFP in interphase yeast cells. The two ends of chromosomes 3 and 6 interact significantly but transiently, forming whole chromosome loops. For chromosomes 5 and 14, end-to-end interaction is less frequent, yet telomeres are closer to each other than to the centromere, suggesting that yeast chromosomes fold in a Rabl-like conformation. Disruption of telomere anchoring by deletions of *YKU70* or *SIR4* significantly compromises contact between two linked telomeres. These mutations do not, however, eliminate coordinated movement of telomere (Tel) 6R and Tel6L, which we propose stems from the territorial organization of yeast chromosomes.

Introduction

Long-range chromosome organization is thought to influence nuclear function, yet little is known about how chromosomes fold in their natural states, and what forces or constraints produce recognizable patterns of chromosome positioning (for review see Dundr and Misteli, 2001; Spector, 2003). Two general types of interphase organization have been described. One is the polarized Rabl configuration, with centromeres and telomeres at opposite poles of the nucleus (for review see Spector, 2003), and the second a domain organization in which individual chromosomes occupy discrete territories that generally do not overlap (Cremer et al., 2001). The Rabl configuration was initially observed in rapidly dividing embryonic and salivary gland nuclei of salamanders (Rabl, 1885), and is prominent in both *Drosophila melanogaster* (Hochstrasser et al., 1986) and plant cells (wheat, rye, barley; for review see Shaw et al., 2002). However, in *Arabidopsis* (Fransz et al., 2002) and in most mammalian cells (Cremer et al., 2003; Spector, 2003) this polarized chromosomal organization, which results naturally from the pulling forces of the anaphase spindle, degrades after telophase. Thereafter, individual chromosomes tend to occupy distinct zones called territories, with variable nearest neighbors. Despite this irregularity in chromosome–chromosome contacts, one can detect tissue-specific distributions of chromosomes in mammalian cells (Parada et al., 2004). Moreover, their relative radial position correlates with gene density on human chromosomes in both lymphocytes and transformed cells (Croft et al., 1999). Nonetheless, the forces that determine chromosome position in interphase nuclei are unknown and no specific mutations have been reported that alter their spatial juxtaposition.

One means for the positioning of chromosomes may be the anchorage of specific chromosomal elements. It is well established in unicellular organisms like yeasts, *Plasmodia* and *Trypanosoma*, that telomeres are grouped in clusters at the nuclear envelope (NE; Funabiki et al., 1993; Scherf et al., 2001). This organization is well-characterized in *Saccharomyces cerevisiae*, where there are five to eight discrete perinuclear foci, each containing five to seven telomeres (Gotta et al., 1996). Moreover, yeast centromeres cluster near the membrane-embedded spindle pole body (SPB; Guacci et al., 1997; Jin et al., 1998; Heun et al., 2001a; Bystricky et al., 2004). Theoretically, these clustering

Correspondence to Susan M. Gasser:susan.gasser@fmi.ch

Kerstin Bystricky's present address is Laboratoire de Biologie Moléculaire Eucaryote/IFR109, Université Paul Sabatier, 31062 Toulouse, France.

Thierry Laroche and Susan M. Gasser's present address is Friedrich Miescher Institute for Biomedical Research, CH-4058 Basel, Switzerland.

Abbreviations used in this paper: 2D, two-dimensional; 3D, three-dimensional; ARS, autonomously replicating sequence; Chr, chromosome; IF, immunofluorescence; MSD, mean square displacement, NE, nuclear envelope; r^c, radius of confinement or spatial constraint; SPB, spindle pole body; Tel, telomere.

The online version of this article contains supplemental material.

The Journal of Cell Biology, Vol. 168, No. 3, January 31, 2005 375–387
http://www.jcb.org/cgi/doi/10.1083/jcb.200409091

events are compatible with a Rabl-like arrangement for yeast interphase chromosomes (Ostashevsky, 2002), in which centromeres and telomeres would be found at opposite poles. However, no imaging study to date has specifically tagged both right and left telomeres of a given yeast chromosome to formally demonstrate a Rabl configuration. A recent cross-linking study suggests that subtelomeric regions of the budding yeast chromosome (Chr) 3 interact preferentially in living cells (Dekker et al., 2002). Because Chr 3 is a small yeast chromosome which bears unusual GC-rich isochores (Bradnam et al., 1999) and active and silent mating type loci, it was unclear whether other yeast chromosomes would yield similar cross-linking results.

Here, we directly examine the organization of chromosomes in vegetatively growing yeast cells, exploring the relationship of this organization to mechanisms that anchor telomeres at the NE. Exploiting two different bacterial repressor proteins with high affinity for integrated operator site arrays (*lac*^{op} or *tet*^{op} arrays), we analyze chromatin structure in vivo at high resolution with live fluorescence microscopy (Belmont, 2001). Past studies have used such tools to examine the dynamics of individually tagged chromosomal loci, revealing rapid and constant, yet spatially constrained movements. Typical loci shift position frequently (0.1–0.5 μm/s) within restricted subnuclear volumes (Marshall et al., 1997; Heun et al., 2001b), characteristics that seem to be conserved from yeast to man. Yeast centromeres and telomeres, on the other hand, move within more tightly restricted zones and remain near the nuclear periphery (Heun et al., 2001b; Hediger et al., 2002). By using GFP derivatives fused to different bacterial repressors (i.e., lacI and tetR), we are able to use similar techniques to study the global folding of chromosomes in vivo, avoiding artifactual trans-interactions between arrays of like repressor molecules (Aragon-Alcaide and Strunnikov, 2000). We further examine the positions of differentially tagged telomeres relative to subnuclear landmarks such as the SPB, the nucleolus and NE.

The right and left telomeres of several budding yeast chromosomes interact frequently, but not stably. The interaction is most pronounced for two small chromosomes, Chr 3 and Chr 6, which have relatively short chromosomal arms of roughly equal length, yet the resulting Rabl-like organization is demonstrated for two other larger chromosomes. Telomere–telomere interactions are compromised in cells lacking the proteins involved in perinuclear anchoring, namely yKu and Sir4p. Nonetheless, even in strains lacking these tethers, the movement of telomeres on opposite chromosome arms is coordinated, which is not observed for telomeres of unlinked chromosomes. We suggest that centromere anchorage and telomere–telomere interactions, together with the general compaction of chromatin into a 30-nm fiber (Bystricky et al., 2004), determine chromosome position in the yeast interphase nucleus.

Results

Nuclear polarity is maintained throughout interphase

To examine chromosome positioning in yeast, we first identified fixed points of reference within the nucleus from which cell-autonomous measurements could be made. The yeast nucleolus, which represents a single large domain of rDNA transcription and processing, occupies a distinct subnuclear territory, adjacent to the NE (Fig. 1 A, CFP-Nop1). Immunofluorescence (IF) on fixed cells maps the nucleolus to a zone opposite the SPB, an integral NE structure that serves as the microtubule-organizing center in yeast (Yang et al., 1989; Fig. 1 B). Time-lapse imaging has shown that the SPB movement is constrained to very small volumes over 5-min intervals, moving far less than a telomere or centromere (Heun et al., 2001b). However, it was not clear when the SPB becomes positioned opposite the nucleolus, nor how long this arrangement persists. To visualize this organization in living yeast cells, we have fused a component of the SPB (Spc42) and Nop1, an abundant RNA-binding nucleolar protein, to GFP alone or to CFP in combination with a GFP-Nup49 fusion that labels nuclear pores (Belgareh and Doye, 1997). Cells were subjected to live time-lapse imaging at 12-s intervals for GFP alone (Video 1, available at http://www.jcb.org/cgi/content/full/jcb.200409091/DC1), or at 3-min intervals for CFP and GFP in combination with capture of the transmission channel using a scanning confocal microscope (Video 2, available at http://www.jcb.org/cgi/content/full/jcb.200409091/DC1). Visual inspection confirmed that normal cell growth was not impaired during or after imaging.

Consistent with IF results, the crescent-shaped nucleolus (Fig. 1 A, CFP-Nop1, red) is found at one end of the nucleus, directly opposite the SPB (Fig. 1 A, 0- and 45-min frames, CFP-SPB in white). Remarkably, the SPB focus is reproducibly positioned on a vector that can be drawn from the nucleolus toward the emerging bud, indicating that nuclear and cellular polarities are linked (Fig. 1, A and B). As cells advance to late G2 phase and the nucleus elongates into the daughter cell, the duplicated SPBs separate, and one migrates back toward the nucleolus in the mother cell. These cells traverse mitosis rapidly (Fig. 1 A, 9 min; Video 2), at which point the two SPBs are found at opposite ends of the extended nucleus and the nucleolus spans the length of the spindle. In early telophase, the duplicated nucleolus splits in two, assuming symmetrical positions in mother and daughter nuclei and in G1 phase, the nucleus rotates slightly such that the nucleolus is again localized opposite the SPB (Fig. 1 A, 15–18 min). Thereafter, the nucleolus remains stably positioned opposite both the SPB and the future or actual site of bud emergence throughout G1 and S phase (Fig. 1 B). Statistical support for this observation, comes from scoring SPB position in cells arrested in late G1 phase: in >80% of the cases the SBP falls within 5° of a perpendicular line extending from the nucleolus to the bud neck (Fig. 1 C). We conclude that the nucleolus maintains a position opposite the SPB, which itself maintains a fixed position throughout interphase.

Further evidence that the nucleus does not rotate continuously in G1 phase, is based on GFP-Nup49 FRAP experiments (Fig. 1 D). We irreversibly photobleached the nuclear pore fluorescence within the NE and monitored fluorescence recovery at time intervals relevant to those used to monitor chromatin dynamics of interphase chromatin (i.e., 1.5–10-s intervals over several minutes). If the nucleus were turning rapidly, we would expect to see the bleached zone move from the plane of focus. This does

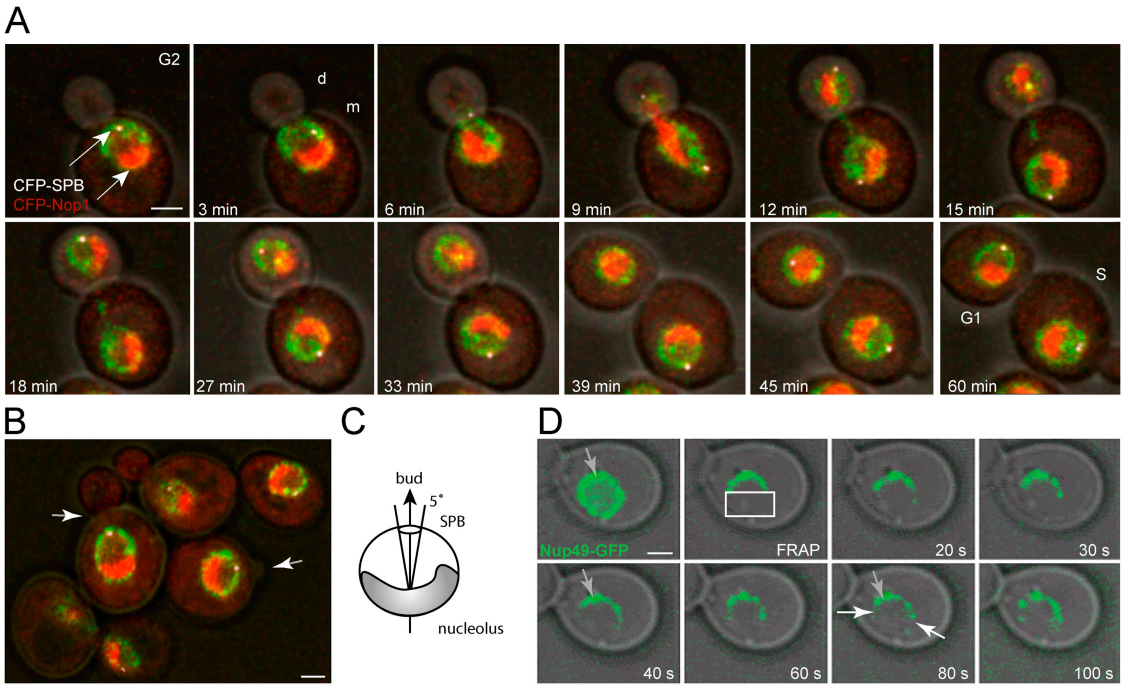

Figure 1. **The yeast SPB and nucleolus are aligned with the site of bud emergence throughout interphase.** (A) Selected frames from a Zeiss LSM510 confocal time-lapse series of GA-2253 yeast cells as they progress through G2, mitosis and G1, show the NE (Nup49, green) and the SPB (white) opposite the crescent-shaped nucleolus (Nop1, red). The CFP-SPB signal was substituted digitally with white to facilitate visualization. See also Video 2. d, daughter cell; m, mother cell. (B) A population of cells tagged as in A, showing the relationship of the nucleolus and SPB to the emerging bud (arrows). (C) Schematic representation of interphase nuclear polarity. (D) GFP-Nup49-labeled pores in G1-phase cells (GA-2197) were bleached (white frame) by confocal laser exposure and epifluorescence/phase images were taken at 10-s intervals thereafter. Pores indicated are either immobile (gray arrows) or slowly diffusing (white arrows). Bars, 1 μm.

not occur (Fig. 1 D). Instead we observe a slow diffusion of pore fluorescence inwards from the edges of the bleached zone, beginning at ~80 s (Fig. 1 D, arrows). We conclude that the global orientation of the interphase nucleus in yeast is quite stable, not only with respect to the SPB, but also with respect to cytoplasmic structures. Nuclear landmarks such as these can thus be used to monitor relative position of chromosomal tags, and rotation of the nucleus can be ruled out as a source of chromatin mobility.

Juxtaposition of right and left telomeres at the nuclear periphery

Previous studies have shown that yeast telomeres are enriched near the nuclear periphery in G1- and S-phase cells, both when detected individually or through repeat sequences (Gotta et al., 1996; Hediger et al., 2002). Nonetheless yeast telomeres are dynamic, shifting irregularly along the NE and occasionally into the nucleoplasm. To explore spatial relationship of pairs of telomeres in vivo we have differentially tagged the two ends of chromosomes 3, 5, 6, and 14, within the most distal unique sequences, such that subtelomeric repeats remain unaltered (Fig. 2 A). We measured distances separating the *lac*^{op} and *tet*^{op} insertions, visualized by the binding of CFP- or YFP-fusions to the bacterial repressors, on three-dimensional (3D) confocal stacks of intact cells (Fig. 2, A and B). The distributions of 3D measurements (n = 60–160 for each telomere pair) are plotted in Fig. 2 (C and D), and the mean distances between tagged sites are summarized in Table I. At a given moment, the left and right telomeres of Chr 3 and 6 coincide or are immediately adjacent to each other (separation in 3D = 0.2 ± 0.2 μm) in 35–40% of the cells measured. Telomere separation for these two chromosomes is clearly skewed to small distances: >75% of the intra-telomere 3D measurements are under 0.8 μm (Fig. 2 C). This is in contrast to the separation of two peripheral but unlinked telomeres (5L and 14R; or 6L and 14L), which follows a near Gaussian distribution around 1 μm (Fig. 2 D). Indeed, if two telomeres on the same chromosome were to have no bias toward interaction, the distribution of distances should be Gaussian over a range from 0.1 to 2 μm, depending on the compaction ratio of the chromatin and the length of chromosomal arms. Separation distances for right and left telomeres of Chr 5 and Chr 14 are also biased toward values <0.8 μm, but unlike Chr 3 and Chr 6, telomeres are immediately adjacent or superimposed in only ~12% of cells.

Chromosomes fold back on themselves in interphase

We next analyzed the relationship of telomere pairs to the centromere by combining the double-tagged chromosomes with staining for the SPB (Fig. 3, A–C). Elsewhere we have established that all centromeres cluster within 200–300 nm of the SPB (Bystricky et al., 2004). By measuring the 3D distance between two telomeric spots and the distance between each telomere and the SPB (Fig. 3, A–C; Fig. S1, available at http://www.jcb.org/cgi/content/full/jcb.200409091/DC1), we deter-

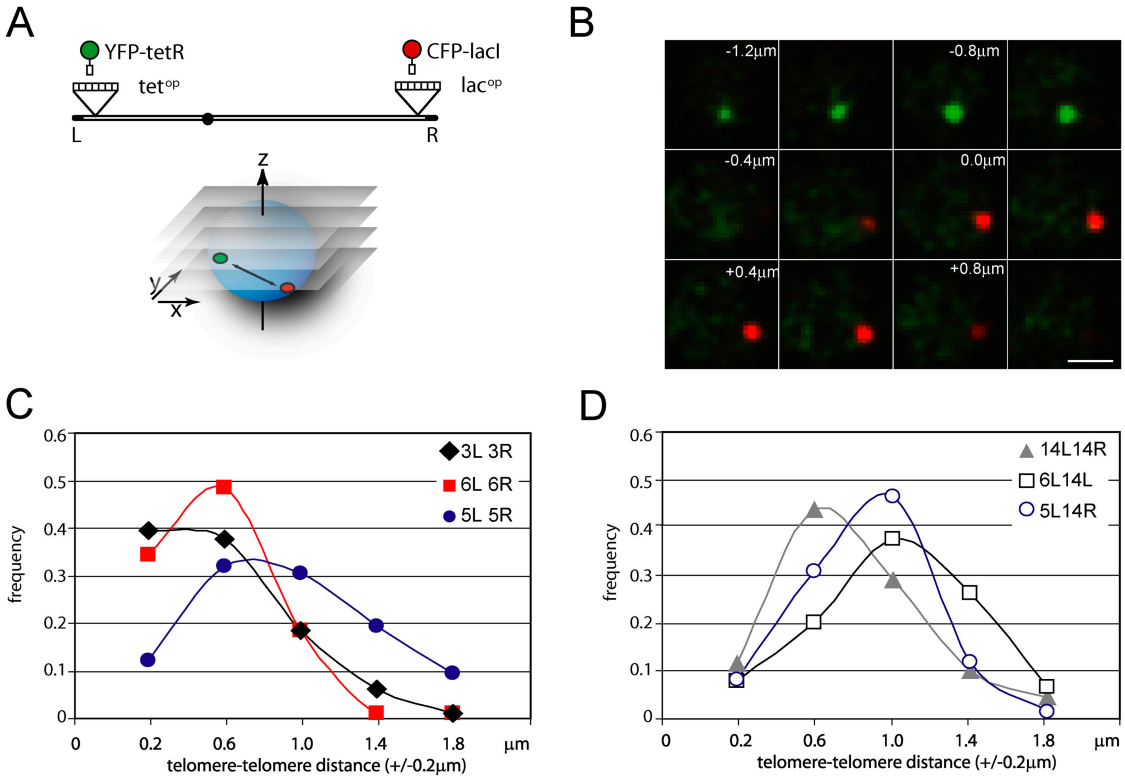

Figure 2. **3D position of telomeres relative to each other in intact cells.** (A) CFP-lacI and YFP-tetR fusions allow visualization of the inserted *lac*^{op} and *tet*^{op} arrays. (B) Image stacks (x-y planes) of 0.2 μm along the z-axis from the Zeiss LSM510 are shown for Tel 5L (CFP, red) and 5R (YFP, green). Bar, 1 μm. (C and D) Distances between the two telomeres in strains GA-2337 (3R3L), GA-2201 (6L6R), GA-2199 (5L5R), GA-2468 (14L14R), GA-2757 (5L14R) and GA-2202 (6L14L). Images of intact fixed cells were acquired in 3D, typically taking stacks of 12–16 focal planes of 0.2-μm intervals along the z-axis. Distributions of distances are plotted by 0.4-μm categories (±0.2 μm).

mine the long-range organization of the chromosome and calculate an angle α that subtends telomere separation. Again, right and left telomeres of Chr's 3 and 6 are frequently juxtaposed (>30% at <0.2 μm, 60–70% at <0.6 μm), whereas the telomere (Tel) 5R and Tel5L separation exhibits greater variability (Fig. 3 D). Importantly, we note that right and left telomeres are almost always more closely juxtaposed to each other than either is to the SPB (Fig. S1). This argues for a fold-back structure that is dominant for Chr's 3 and 6, and statistically significant for Chr 5 (see below).

Table I. **Average 3D telomere–telomere distances**

	Intact cells			Fixed cells (after immunofluorescence)		
	Average distance	stdev	*n*	Average distance	stdev	*n*
	nm			*nm*		
3R 3L	537	345	56	608	429	160
5R 5L	920	430	70	900	465	133
6R 6L	529	251	153	629	322	111
14R 14L	820	410	144			
14L 6L	1,020	400	98	994	315	48
14R 5L	910	520	58			

Separation of the indicated telomeres as monitored in 3D through either live fluorescence (intact cells) or on formaldehyde fixed cells immunostained for the SPB (fixed cells).

By triangulation we determined the angle α at between right and left chromosome arms, using the SPB signal as the apex. The distribution of these angles is summarized in Fig. 3 E. Mean angle values for each chromosome are 31° ± 32° for Chr 3, 38° ± 26° for Chr 6, and 44° ± 29° for Chr 5. This large variability is inherent to the dynamic nature of telomeres and does not represent different subpopulations (see below). It is noteworthy, however, that among the three chromosomes studied, very few angles are >90° and none are >110°, and ~50% of Chr 3 and Chr 6 arms meet at angles <30°. If telomeres were on 1 μm long arms randomly distributed on the surface of a sphere around a fixed point (the SPB), the subtending angles would have Gaussian distribution around 60°. We can conclude, therefore, that the fold-back organization of Chr's 3 and 6 is statistically significant, reflecting right and left telomere interaction. Chr 5 appears also nonrandomly folded (>70% of the angles are <60°), although Tel5R-5L interactions are less frequent. Finally, the average distance separating Tel14L and 14R (Table I) is less than the one separating Tel 5L and 5R, arguing that Chr 14 also assumes a Rabl-like organization.

Right and left telomere interactions are favored by perinuclear constraints

Two parameters may influence telomere–telomere interaction: the length of chromosome arms and their association with the NE. Indeed, the arms of Chr 3 and 6 are both short and of nearly

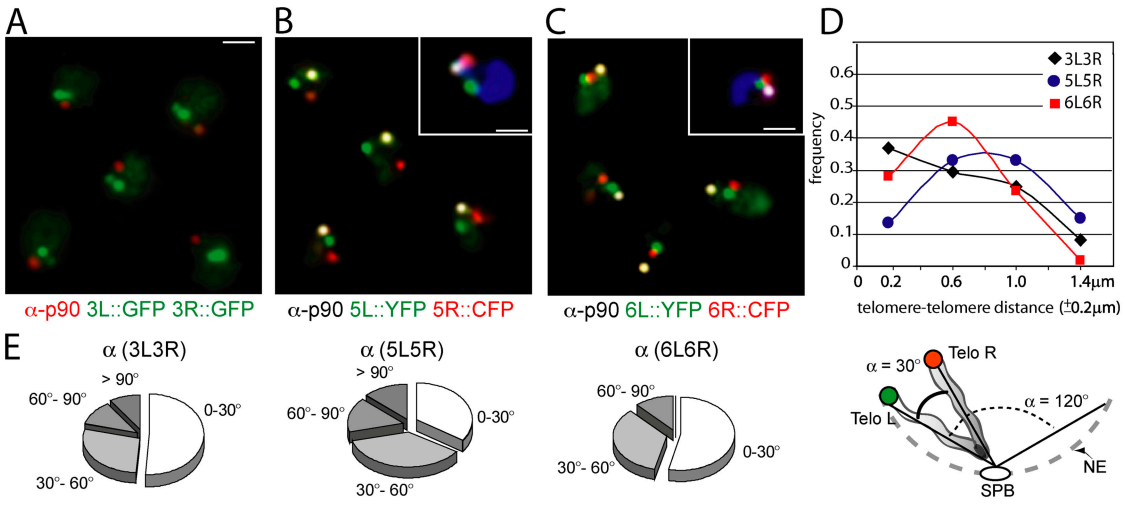

Figure 3. **Chr 3 and Chr 6 form whole chromosome loops.** Epi- and IF of G1-arrested haploid cells: (A) GA-2195 (SPB, red; 3L::GFP, green; 3R::GFP, green); (B) GA-2201 (SPB, white; 5L::YFP, green; 5R::CFP, red); (C) GA-2199 (SPB, white; 6L::YFP, green; 6R::CFP, red). An example of four color images with the Nop1 channel in blue is given in the insets of B and C. Bar, 1 μm. Shown are maximal projections of 10 0.25-μm z-sections. (D) Distance frequencies between the two fluorescent markers (in 0.4 μm categories ± 0.2 μm) for the telomere pairs of Chr 3 (black diamonds), Chr 5 (blue circles), and Chr 6 (red squares). (E) Distribution of the angles α calculated by triangulation of the 3D measurements for all individual cells examined in G1 and S-phase cells. Schematic representation of a folded chromosome and intervening angle α between two chromatids.

equal lengths (3R/3L = 115 kb/200 kb and 6R/6L = 122 kb/148 kb), which is not true for either Chr 5 or 14. However, short, equal arm length is not alone sufficient to favor interaction of chromosome ends: the chromosomal arms of Tel 5L and Tel 14R are also short and of equal length (152 and 150 kb, respectively), yet these ends are separated on average by ~1 μm (Table I). Thus, chromosome arm length probably only favors telomere–telomere interaction when the arms are physically linked.

We next examined whether the efficiency with which each telomere is found at the GFP-Nup49-tagged NE, correlates with the efficiency of their interaction in trans. We scored telomere position relative to three equal zones of the nucleoplasm, focusing on the peripheral-most zone, which has a width of only 0.184 times the radius (Fig. S2, available at http://www.jcb.org/cgi/content/full/jcb.200409091/DC1). For all except Tel5R, we monitor a significant enrichment in this zone, with the following hierarchy: Tel14R > 5L ≈ 6R > 14L ≈ 3R ≈ 6L > 3L (Table II). Only Tel5R has a near-random distribution in G1-phase cells. Similarly, nontelomeric loci, such as *MAT***a**, which sits in the middle of Chr 3, or origins of replication located 73 or 437 kb from the nearest telomere (autonomously replicating sequence [ARS] 607 or ARS1, respec-

Table II. **Telomere position and dynamics in G1-phase cells**

Insertion	kb from telomere	Strain GA–	Position (in G1 phase)				Dynamics (in G1 phase)				
			% zone I	Enrichment (obs/random)	*n*	P value	Velocity (nm/s)			D ($\times 10^{-11}$ cm^2/s)	r^c (μm)
							Average	*Min*	*Max*		
3L	17	2193	43	1.3	181	5.8×10^{-3}	73	59	87	1.8	0.40
3R	20	2194	51	1.5	122	3.5×10^{-5}	90	73	107	2.5	0.40
*MAT***a**	111	2196	19	0.6	162						
5L	10	2197	60	1.8	126	2.2×10^{-10}	96	62	130	6.2	>0.7
5R	17	2198	35	1.0	189	0.62	110	80	141	6.9	>0.7
6L	16	2200	49	1.5	122	2.4×10^{-4}	99	80	118	2.8	0.40
6R	13	1459	58[a]	1.7	110	4.1×10^{-8}	98	78	119	3.2	0.47
ARS607	73	1461	37[b]	1.1	322	0.16					
14L	19	1985	54[a]	1.6	257	2.1×10^{-12}	91	65	118	2.3	0.50[c]
14R	6	2468	71	2.2	138	2.0×10^{-20}					
ARS1/Cen4	437	1324					118	87	137	6.9	0.63

Individual telomere position reflects their distribution among three zones of equal surface (see Fig. S2); values >33% in zone 1 represent enrichment in the peripheral-most zone. *n* is the number of G1-phase cells analyzed. *t* test was performed to compare distributions with a random distribution (P values for 95% confidence level are shown). Individual telomere dynamics were analyzed by 2D confocal live microscopy as described in Figs. 4 and 5. The average velocity of each telomere is obtained by dividing the total path length by the total time period. The diffusion constant (D = MSD/Δt) is proportional to the initial slope of the abs MSD plot (1.5-s interval) and the radius of constraint is determined from its plateau and the formula maximal MSD = 4/5 $(r^c)^2$.

[a]From Hediger et al. (2002).

[b]From Heun et al. (2001b).

[c]r^c for Tel 14L is determined at Δt = 60 s, because the tendency to move horizontally along the NE distorts the r^c value for this telomere.

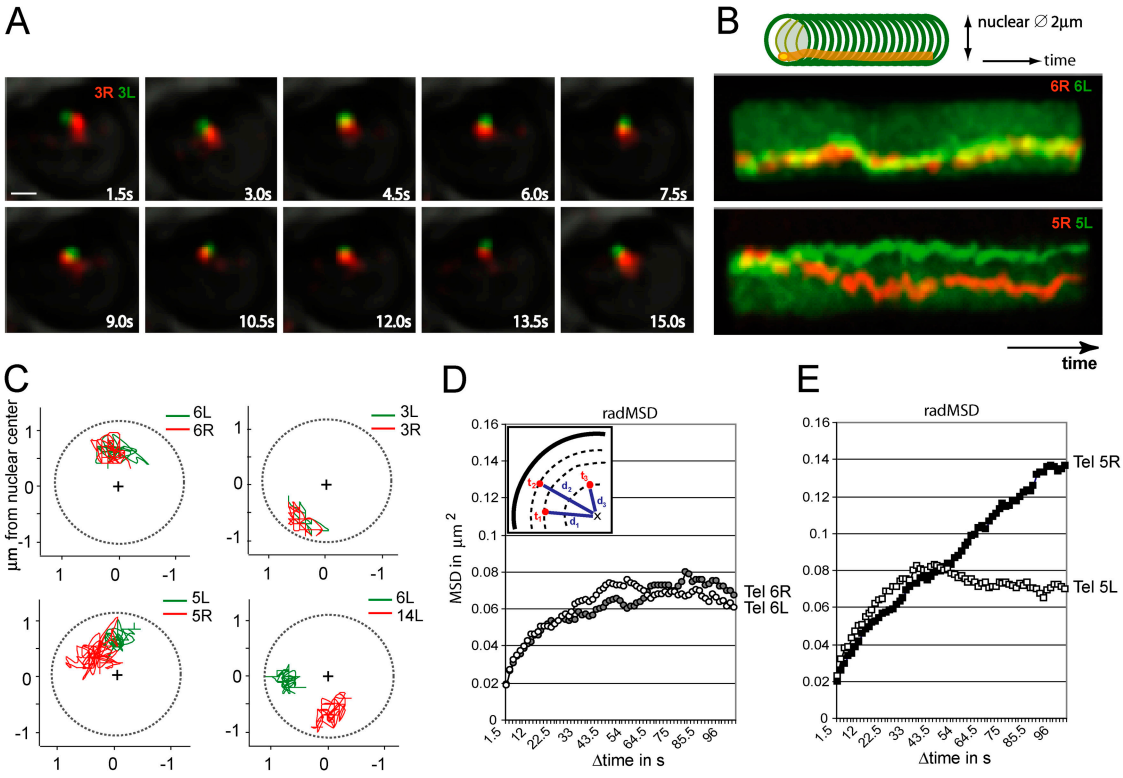

Figure 4. **Live imaging of telomere dynamics.** A Zeiss LSM510 confocal time-lapse microscopy (2D) was performed on double-tagged Chr 3, 5, 6, and 14 taking frames every 1.5 s, by adjusting the plane of focus when necessary (see time-lapse series as Videos 3–6). (A) Representative sequence of frames taken at 1.5-s intervals in 2D of GA-2337, 3R::CFP (red), 3L::YFP (green). Bar, 1 µm. (B) Telomere tracks over time: 100 sequential images from 2D time-lapse series are displayed orthogonally, rotated such that the time axis (z) is horizontal. Top panel: GA-2201 6L::YFP (green), 6R::CFP (red) and bottom panel: GA-2199, 5L::YFP (green), 5R::CFP (red). TetR-YFP also produces the diffuse green background. (C) Examples of telomere tracks over 100 frames of 2D time-lapse videos after alignment of interpolated nuclear centers (YFP, green; CFP, red). The dotted circle represents an idealized nuclear circumference (Ø = 2 µm). (D) Radial MSD for telomeres 6R and 6L and 5R and 5L obtained using d = distance between one fluorescent telomere spot and the center of the nuclear background fluorescence for each frame as a function of the time interval (inset, for t = 1.5–101.5 s).

tively), are either randomly distributed or depleted from the periphery (Table II). Although the well-paired telomeres (those of Chr 3 and 6) tend to be perinuclear, from these measurements one can draw no simple correlation between the efficiency of NE interaction and telomere interaction.

Two color time-lapse imaging reveals constraints on telomere movement

Every measurement on a fixed cell is, of course, a snapshot of a dynamic chromosomal state, and even telomere–telomere interactions are not static. To monitor directly how stable telomere interactions are, we used live time-lapse imaging to follow the relative movement of differentially tagged telomeres. Up to 250 sequential two-channel (CFP-YFP) confocal images were acquired at 1.5-s intervals without detectable impact on cell-cycle progression. For each strain, we analyze 8–12 independent two-dimensional (2D) time-lapse series (totaling 35–58 min each) of G1-phase nuclei, after the tagged foci by adjusting the focal plane. Representative sequences and videos are shown in Fig. 4 and Videos 3–6, available at http://www.jcb.org/cgi/content/full/jcb.200409091/DC1.

Projection of the paths taken by the individual telomeres onto one plane shows that movements are not only restricted to a fraction of the total nuclear volume, but that the tracks of the Tel 3R-3L and Tel 6R-6L coincide extensively (see examples from typical videos; Fig. 4 C). Tel 5R-5L move in close proximity but with little overlap. The juxtaposition does not arise from the methodology used, because movements of unlinked telomeres (Tel 6L-14L) are distinct and uncoordinated, consistent with measurements at fixed time points (Table I). By summing all individual steps over the total time and dividing by the period elapsed, we calculate the average velocity of each individual telomere (Table II). We find that all telomeres except Tel 5L and 5R are significantly less mobile than the tagged centromere-proximal *ARS1* locus.

Assuming that chromatin motion resembles a constrained random walk (Marshall et al., 1997), locus mobility can also be characterized by plotting its mean square displacement (MSD or $<\Delta d^2>$) over increasing time intervals. Unconstrained diffusion gives a linear relationship between increasing time intervals and the square of the distance travelled by a particle during that time, where $\Delta d^2 = (d(t)-d(t+\Delta t))^2$ (Berg, 1993; Hediger et al., 2004). The MSD curve for chromatin with a spatially constrained diffusion process generally reaches a plateau by $\Delta t > 50$s. This analysis is highly robust because Δt intervals are pooled from all videos of a given strain.

If we monitor movement as displacement relative to the nuclear center or the nearest point on the NE (d = distance be-

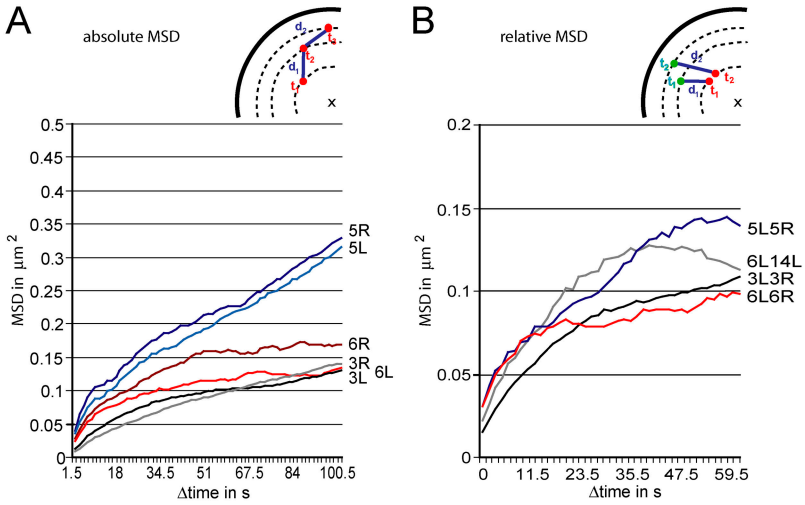

Figure 5. **Looping of short chromosomes correlates with reduced telomere mobility.** (A) Absolute MSD calculated using the 2D videos as described in Fig. 4 for telomeres 5R, 5L, 6R, and 6L using d = actual distance from any one time point to all others (see diagram; for t = 1.5–101.5 s) after nuclear alignment. (B) Relative MSD calculated using d = distance between two telomeres at all possible time intervals (see diagram; for t = 1.5–61.5 s), for the indicated pairs of telomeres.

tween one fluorescent telomere spot and the center of the nuclear background fluorescence, cf. Heun et al., 2001b), the resulting MSD curve reflects the dynamics of a given locus relative to the nuclear periphery (radial MSD or radMSD; Fig. 4 D). RadMSD curves show that the dynamics of telomeres 5L, 6R and 6L are nearly equally restricted relative to the NE, whereas Tel 5R moves without constraint relative to the NE (Fig. 4, D and E). The two telomeres of Chr 3 exhibit NE-constrained movement very similar to Chr 6 (unpublished data). By comparing telomere movements and paths, we conclude that path superposition of right and left telomeres correlates positively with constraint relative to the NE, even though precise distance from the NE may vary. Thus, constrained movement relative to the periphery, whether directly at the NE or not, does correlate with contact between telomeres.

Absolute and relative constraints on telomere dynamics

A more accurate analysis of spatial constraint is based on measurements that reflect the actual distances covered from any one time point to all others (i.e., rather than distances relative to the periphery; Fig. 5 A), after an alignment of nuclear centers to eliminate background drift. These d values were then subjected to the similar MSD analysis (here called absolute or absMSD) for both telomeres of Chr 3, 5, and 6. When absolute step sizes are the basis of the curve, the radius of confinement or spatial constraint (r^c) determines the plateau of the MSD curve (Ma × MSD). For our geometry, this dependence is Ma × MSD = 4/5 $(r^c)^2$ (J. Dorn and Neumann, F., personal communication). Solving for r allows us to calculate the radius of confinement from experimental MSD curves. This analysis shows that Tel 5R and Tel 5L are relatively mobile and do not reach a plateau, yet from the radial analysis we know that Tel 5L tracks along the NE (Fig. 4 E and Fig. 5 A). By contrast, movements of Tel 6R, 6L, 3R, and 3L, show clear spatial constraint and r^c values ranging from 0.40 to 0.46 μm.

The initial slope of the absMSD plot is proportional to the maximal diffusion constant (D = MSD/Δt). These slope values confirm that Tel 5R and 5L are more dynamic than other telomeres, with diffusion rates similar to those of the centromere proximal *ARS1* locus (6.9×10^{-11} cm^2/s; Table II). Although Tel 5R and 5L are more mobile than other telomeres, we show here that they move in a paired manner, by scoring the relative separation of the telomere pairs throughout >2,000 frames (Fig. S3, available at http://www.jcb.org/cgi/content/full/jcb.200409091/DC1). Distances separating telomeres derived from time-lapse series confirm the values determined in 2D and 3D at fixed time points (Figs. 2 and 3): Tel 6R-6L and Tel 3R-3L are tightly juxtaposed, with 32–37% of all distances ≤0.2 μm, and >50% ≤0.4 μm. Strikingly, >60% of the separation values for Tel 5R-5L are ≤0.5 μm, whereas the separation of two unrelated telomeres (i.e., Tel 6L-14L) is <0.2 μm in only 5% of all frames. This confirms that Tel 5R-5L are adjacent although rarely interacting.

To quantify the freedom of movement that two telomeres have relative to each other, we plot the change of distances separating the telomeres as a function of t. In this "relative MSD" analysis, d is defined as the distance between two telomeres at any given time point (Fig. 5 B, relative MSD; Berg, 1993; Marshall et al., 1997; Vazquez et al., 2001). These MSD plateaus confirm that all telomere pairs tested undergo obstructed diffusion, yet the values for linked telomere pairs are grouped around $<\Delta d^2>$ = 0.1–0.14 μm^2. This suggests that two different telomeres move more freely relative to one another than do two identical centromere proximal sites monitored in a diploid cell (for *LEU2*/Cen3, $<\Delta d^2>$ = 0.06 μm^2; Marshall et al., 1997). It is nonetheless noteworthy that even two unlinked telomeres (Tel6L-14L), which are separated by roughly 1 μm in the nucleus, show a relative radius of constraint of r^c = 0.25 μm. From this one can conclude that, independent of their pairing efficiency, telomeres assume fairly fixed positions in interphase nuclei.

Nuclear order is disrupted in the absence of yKu70 or Sir4

We have recently established that yeast telomeres are bound at the NE through dual pathways. One requires Sir4 and the other yKu (Hediger et al., 2002; Taddei et al., 2004). To examine directly whether the observed fold-back organization of chromosomes depends on telomere anchoring, we analyzed the posi-

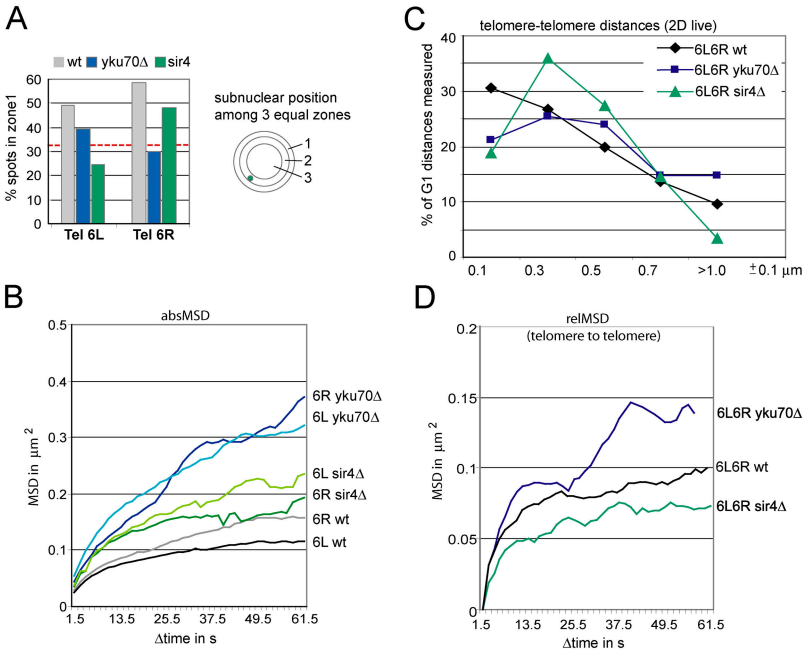

Figure 6. **Nuclear order is disrupted in the absence of yKu70p or Sir4p.** Mobility, telomere–telomere separation, and telomere anchoring of Chr 6 are compared in wild-type, *yku70*, and *sir4* cells. (A) Positions relative to the NE in wt (gray), *yku70* (blue), and *sir4* (green) strains of GFP tagged telomeres 6L and 6R mapped to zone 1 (as described in Fig. S2 and Table II). The number of G1-phase cells analyzed and the 95% confidence values (P) for the *t* test between random and test distributions for 6L are: 122, $P = 2.5 \times 10^{-3}$ for 6L wt; 81, P = 0.6 for 6L yku70; 57, $P = 4.2 \times 10^{-5}$ for 6L sir4; for 6R data see Hediger et al. (2002). (B) Absolute MSD was calculated using the 2D videos as described in Figs. 4 and 6 (for t = 1.5–61.5 s). (C) Frequencies of distances from 2D time-lapse series between the two tagged loci are displayed as a function of 0.2-μm intervals (±0.1). (D) Relative MSD calculated using d = distance between telomeres 6R and 6L at all possible time intervals (for t = 1.5–61.5 s).

tion and dynamics of Tel 6L and 6R after disruption of either *YKU*70 or *SIR4*. In the absence of the yKu complex, Tel 6R is delocalized from the periphery (Hediger et al., 2002) becoming randomly distributed in the nucleus, whereas Tel 6L anchoring is only slightly diminished (Fig. 6 A). In contrast, *sir4* deletion releases Tel 6L, but not Tel 6R (Fig. 6 A). Confirming the redundancy of the anchoring pathways, we note that all telomeres analyzed to date lose their perinuclear position in double *sir4 ku70* mutants (Hediger et al., 2002; unpublished data). The mobility of Tel 6R and 6L also increases in these mutants, as monitored by live time-lapse imaging and absMSD analysis (Fig. 6 B). Plateau heights correspond to increases in average r^c from 0.38 or 0.43 μm in wild-type cells, to 0.5 μm in the *sir4* mutant and >0.6 μm in *yku70* cells.

We next asked whether the relative distance between the two telomeres changes significantly in these mutants. The separation between telomere pairs was monitored for mutant and wild-type cells as a function of time (Fig. 6 D). In both *yku70* and *sir4* mutants, Tel 6L and 6R show significantly greater separation than in wild-type cells (*t* test $P < 0.003$, *yku70*, and $P < 0.005$ for *sir4*). In the mutants <23% of the distances measured are ≤0.2 μm, as compared with >30% in wild-type cells. Because the two arms of Chr 6 are short, a 25% increase of the mean distance between the two telomeres corresponds to a large change in the angle between the two chromatids (Fig. 3 E). The average angle α increases from 39° to 48°, which is larger than that observed for Chr 5 in a wild-type strain (44°). Because centromere clustering near the SPB is unaffected by either the *yku70* or *sir4* deletion (unpublished data), we conclude that the fold-back organization of Chr 6, monitored as telomere–telomere proximity, is severely disturbed when either telomere loses its perinuclear anchoring.

In summary, the loss of yKu or Sir4p should make Chr 6 behave like Chr 5 (i.e., one telomere moves freely and the other is anchored; Fig. 8). Therefore, we plotted the relative MSD between Tel 6L and 6R in the mutant strains (Fig. 6 D), to score their loss of coordination. Indeed, the relative MSD plateau for Tel 6R-6L in the *yku* mutant is higher, similar to that scored for Tel 5R-5L in a wild-type background and consistent with increased mobility of one end (Fig. 5 B). Nonetheless, the plateau is still quite low, as it is in the *sir4* background, suggesting that the ends of a given chromosome preserve a territorial inertia even though they interact less frequently.

Coordinated chromosome dynamics can occur independent of telomere interactions

Do linked telomeres move in a coordinated manner, or simply show constraint relative to each other? To address this we acquired time-lapse videos in 3D (7-image stack of a 300-nm step size) capturing double-tagged telomeres at two wavelengths on the confocal microscope (Fig. 7). Cellular integrity is confirmed by following the imaged cell through the subsequent mitosis. Coordinates of the center of the fluorescent spots were obtained using the IMARIS software, and the nuclear center is interpolated from the YFP-tetR background signal. The nucleus and spot positions for Tel 6L-6R and for Tel 6L-14L were then reconstructed in 3D (Fig. 7, A–C, shown here as projections onto the x, y, and z planes over time). Tel 6L-6R appear frequently, but not always, closely juxtaposed. Even when not juxtaposed, they seem to move in a coordinated fashion, which is not true for 6L and 14L.

The degree to which movement is coordinated can be assessed by a correlation coefficient c (see Materials and methods; no correlation = 0, identical movement = 1). Direction cosines were determined for every vector joining two neighboring points of two separate trajectories, and the mean of Pearson's correlation coefficients (c) in each direction was determined. This was performed both for 2 color 2D and 3D time-lapse series. The movements of Tel 6R-6L have a mean corre-

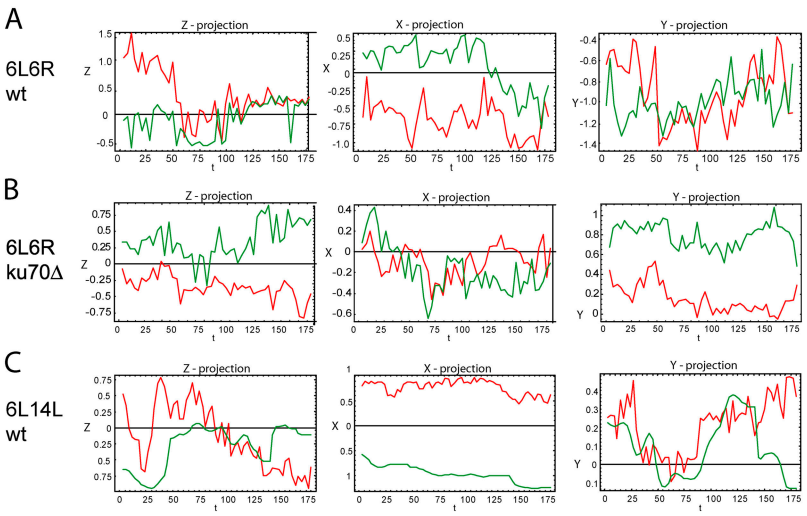

Figure 7. **3D and two-color fluorescence time-lapse imaging of telomere dynamics.** Time-lapse microscopy in 3D (one 7-plane stack every 3 s) was performed on GA-2201 (A), GA-2805 (B), and GA-2202 (C) as described in Materials and methods. Coordinates of both telomeres are plotted in x, y, and z against time. (A and B) Tel 6L::YFP (green) and Tel 6R::CFP (red) in wt (A) and *yku70Δ* (B). (C) Tel 6L::YFP (green), Tel 14L::CFP (red).

lation coefficient of 0.39 in 3D (0.26 in 2D), indicative of closely coordinated movement. Confirming our methodology, we found that two tags on the same telomere gave correlation coefficient of 1 (unpublished data). In contrast, Tel 6L-14L movements show no significant coordination (correlation coefficients of 0.03, for a 3D time-lapse series). Thus, the 6R-6L telomeres move with significant coordination over time, whereas unlinked ends do not.

Similar analysis was performed in strains bearing disruptions of *YKU70* or *SIR4*, which compromises both anchoring and telomere–telomere interactions (Fig. 6). Strikingly, however, in *yku70* and *sir4* mutants the Tel 6R-6L correlation coefficients are ~0.15, which is still half the coordination detected in wild-type cells. In the case of the *yku70* mutant, the 3D time-lapse analysis of Tel 6R and 6L trajectories projected onto x, y, and z planes, suggests a low but detectable degree of coordination in the mutants (Fig. 7 B). We predict that this residual coordination in chromosome dynamics can be attributed to their physical contiguity, i.e., that they represent two ends of a single chromosome. The release of one telomere from the NE and the ensuing drop in telomere interaction nonetheless does lead to a significant increase in unlinked movement.

Discussion

Using high resolution microscopy techniques on living budding yeast cells we establish that the anaphase polarity of chromosomal organization is maintained in nuclei despite the continuous dynamic movement of interphase chromatin. Furthermore, our analysis of position and movement of multiple pairs of budding yeast telomeres in wild-type and mutant strains, shows that right and left telomeres of Chr 3 and Chr 6 interact in a reversible, but highly significant manner. This is the first study in which contact between specific yeast telomeres has been documented by either fixed or live microscopy. These interactions, coupled with the stable polarized clustering of centromeres near the SPB, provides a direct demonstration that yeast chromosomes can assume a looped, Rabl-like organization. Even Chr 5 and 14, whose telomeres interact less frequently, appear to fold-back upon themselves, arguing that a combination of telomere anchoring and trans-interactions contribute to spatial organization (Fig. 8).

The Rabl-like arrangement that we document in budding yeast persists throughout interphase, until the mitotic spindle actively alters chromosome position. A second documented instance of chromosome clustering involves all telomeres during the "bouquet" stage before pachytene in meiotic prophase (Scherthan, 2001). In budding yeast this clustering is mediated by a sporulation-specific protein scNdj1 (Trelles-Sticken et al., 2000), which has no known function in mitotically dividing cells. Similarly, the fission yeast protein spTaz1 mediates meiotic but not mitotic, telomere clustering, a phenomenon that involves telomere anchoring at the SPB (Cooper et al., 1998).

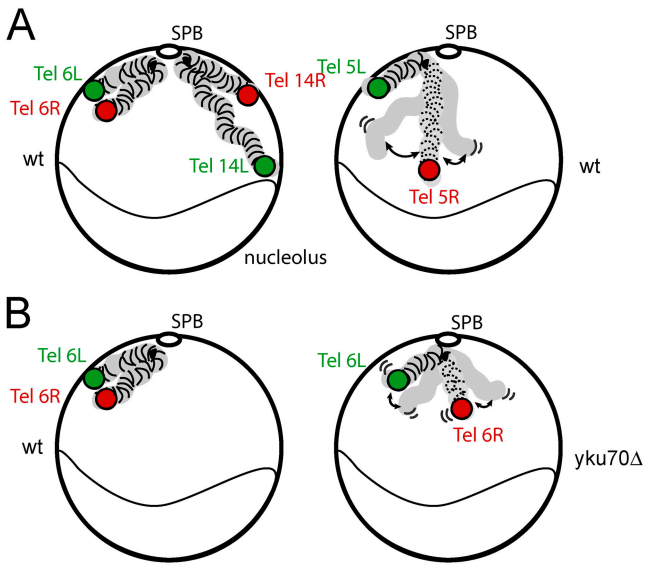

Figure 8. **Schematic representation of a Rabl-like chromosome organization in yeast.** (A) In wild-type cells, short chromosomes with equal length arms, such as Chr 6 and Chr 3, form loops through telomere interactions. Other chromosomes fold back less rigidly. This is more pronounced when both telomeres are anchored in the NE, which is not the case for Chr 5. (B) Nuclear order is disrupted by deletion of *yku70* as the telomeres of Chr 6 detach from the NE and become more mobile.

Multiple elements constrain chromatin mobility to help define chromosome position

We provide novel evidence that long-range interactions between telomeres can be altered in vegetatively growing yeast by interfering with the telomere-associated proteins yKu and Sir4p. These same factors are directly involved in the anchorage of yeast telomeres to the NE. Indeed, silencing-incompetent forms of each protein are sufficient to relocate an otherwise internal locus to the nuclear periphery (Hediger et al., 2002; Taddei et al., 2004). Importantly, the disruption of anchorage at just one end of Chr 6 significantly reduces telomere–telomere interaction (Fig. 7). Correlation analysis of movement in 3D argues that despite their separation, Tel 6R and 6L continue to move in a partially coordinated manner in these *yku70* or *sir4* mutant cells. Because unlinked telomeres do not behave in a similar fashion, we conclude that not only direct interaction, but the contiguity of the chromosomal fiber influences chromatin movement, even though telomeres are separated by several hundred kilobases and a kinetochore.

It has been questioned whether the notion of chromosome "territories" is appropriate for yeast due to the relatively large r^c monitored for individual loci (r^c = 0.5–0.65 μm) and the small size of the yeast nucleus (nuclear radius = 1 μm). The movement we document here indicates that two linked telomeres move in a partially coordinated manner, thus providing a quantifiable parameter for a "chromosomal territory". In contrast to this, a 16-kb ring of chromatin released from its chromosomal context by an inducible recombinase, traverses the nucleoplasm freely and randomly, moving in all directions ($r^c \geq 0.8$ μm for the ring vs. 0.6 μm for the chromosomal locus; Gartenberg et al., 2004). The unconstrained movement of this ring further stresses the impact of chromatid contiguity both on the relative positioning of linked telomeres and on general chromosome positioning in interphase nuclei. In conclusion, we propose that chromosome position is defined by three types of constraint: the contiguity and compaction of the chromosomal fiber, sites of anchorage to less mobile nuclear landmarks (centromeres to the SPB and telomeres to the NE) and finally, reversible interactions between right and left chromosome ends.

Our data strongly support the looped Chr 3 model proposed from an assay that scores the efficiency of cross-linking in vivo (Dekker et al., 2002). Chr 3 is unique among yeast chromosomes in that it carries three homologous mating type loci that participate in a gene conversion event required for mating type switching. Chr 3 also has unique, strongly pronounced GC-rich "isochores" of 30–50 kb (Bradnam et al., 1999), which are not found on the other chromosomes analyzed here. It is conceivable that the folded structure of Chr 3 reflects its propensity for recombination between *MAT* (on the right arm) and *HML* (on the left arm) in MATa cells. However, because Chr 6 forms a whole chromosome loop as efficiently as Chr 3, these Chr 3-specific features are unlikely to be critical for its folding pattern in vivo. We note that the interactions of telomeres on Chr 3 and 6 may well be aided by the fact that these two small chromosomes have similar arm lengths and compaction ratios (Bystricky et al., 2004). Conversely, one might assume that grossly different chromosome arm lengths limit pairing. Finally, we note that chromatid arm length is not a sufficient criterion to determine stable pairing events, because the telomeres of 5L and 14R do not interact despite the equal length of these chromosome arms.

Extended sequence homology is not critical for telomere pairing

Does sequence homology contribute to selective telomere–telomere interactions? It was suggested that transient contact between homologues, or chromosome "kissing" events, would facilitate homology searches in meiotic prophase (Kleckner and Weiner, 1993; Pryde and Louis, 1999). One might imagine that once in contact, sequence homology could in turn promote more stable interactions in trans through ligand binding. Such trans-interactions have been proposed to facilitate silencing, but also are thought to help coordinate the timing of replication of right and left telomeres in budding yeast (Raghuraman et al., 2001). Our study, however, demonstrates that the selective interactions of the Tel 3R and 3L and Tel 6R and 6L does not result simply from sequence homology. Neither pair of telomeres shares any homology other than the universal TG-rich and STR/core X element repeats. Moreover, a pair of telomeres that shares >90% homology over 16 kb (Tel 6L and 14L), almost never interact despite the presence of highly conserved Y' elements. Consistently, entire chromosomal homology also has little impact on pairing: in a yeast strain that serendipitously contains a duplication of the double-tagged Chr 3 (bearing Tel 3R-tet^{op} and 3L-lac^{op} sequences) the two homologous chromosomes are far apart within the nucleus and each forms a separate fold-back structure (unpublished data).

Heterochromatin factors anchor telomeres and contribute to trans-interaction

In budding yeast, a strong candidate for contributing to telomere–telomere interactions could be silent chromatin itself. Silencing efficiency, like the availability of Sir proteins and telomere–telomere pairing, varies from end to end (Pryde and Louis, 1999). Sir4p, a 174-kD protein bears a COOH-terminal coiled-coil domain that is necessary for homo-dimerization as well as interaction with Sir3, Rap1, and yKu (for review see Gasser and Cockell, 2001). The Sir4 COOH-terminal domain has often been compared with nuclear lamins in higher eukaryotes, although Sir4 requires another perinuclear protein, Esc1p, or yKu to ensure its anchoring (Taddei et al., 2004). To test rigorously whether or not subtelomeric heterochromatin directly influences pairing, it will be necessary to compare the efficiency of native telomere repression and the efficiency of native telomere interaction systematically in a single strain background. Whereas *yku70* mutations compromise telomeric silencing, they do not impair mating type silencing, suggesting that reduced interactions do not significantly disrupt the repressive state.

In analogy to Sir4p, HP1 has been proposed to mediate interactions between repressed domains in higher eukaryotes in

trans (Ryan et al., 1999). However, delocalization of HP1 can occur in mammalian cells without the disruption of the chromocenter (Peters et al., 2001). The elimination of Sir4 and yKu oblate telomere associated silencing, much like spTaz1, which is required in fission yeast both for telomere-associated silencing (Kanoh and Ishikawa, 2001) and meiotic clustering. Surprisingly, however, loss of mitotic clustering is governed by the fission yeast RNAi machinery, not Taz1, and mutation of this ironically does not derepress subtelomeric silencing or perinuclear anchorage (Hall et al., 2003). Therefore, although subsets of heterochromatin components may contribute to long-range chromosomal contacts, the loss of interactions in trans, is not necessarily correlated with changes in repression status. Rather, critical components for telomere–telomere interactions, among which may figure cohesin molecules, may simply associate with heterochromatin, participating to different degrees in both repression and trans-interactions (Partridge et al., 2002).

Limited chromosomal mobility can define a territory

Besides specific patterns of chromosome folding and centromere/telomere positioning, we provide evidence that the coordinated movement of the two distal regions of a yeast chromosome is compromised by mutation. We envision this coordinated movement as a sort of "chromosomal inertia," which reflects the tendency of a chromosome to move as one body, even when specific interactions are compromised. Given the mass of a mammalian chromosome, if similar coordination occurs, then this alone could account for the infrequency with which human chromosomes change their territorial distribution (for review see Spector, 2003). Reproducible positioning and limited mobility of chromosomal domains has been documented as well for *Drosophila* cells (Marshall et al., 1996, 1997; Vazquez et al., 2001). We propose that the general inertia of whole chromosome territories in higher eukaryotic cells, may be linked to a phenomenon we quantify here—that of chromosome-wide coordination of constrained movement.

Materials and methods

Plasmid, strains, and yeast methods

Plasmid used to integrate the *tet* or *lac* operators and repressors were as described in Bystricky et al. (2004). PCR-amplified genomic fragments with the indicated SGD coordinates were used for insertion: 15160–15773 (Tel3L), 294892–295241 (Tel3R), 9645–11059 (Tel5R), 558701–559863 (Tel5L), 16431–17993 (Tel 6L), 256581–256893 (Tel6R), 18832–19853 (Tel14L), 778324–779355 (Tel14R), and 197194–196910 (*MAT*). Unique restriction sites were used to linearize the plasmids for integration, which was verified by colony PCR and pulsed field electrophoresis. LacI-GFP and tetR-GFP or tetR-YFP and the lacI-CFP fusions were introduced by integration of pGVH40 or pGVH30

Table III. **Yeast strains used in this study**

Name	Parent	Genotype (parent or relevant modifications)	Reference
GA-180	=W303-1A	*MAT***a** *HML*α *HMR***a** *ade2-1 can1-100 his3-11,-15 leu2-3,-112 trp1-1 ura3-1*	
GA-1320	GA-180	*his3-11,-15::HISp-GFP-LacI-HIS3, nup49::NUP49-GFP*	Heun et al., 2001a
GA-2254	GA-180	*ade2-1::URA3p-tetR-GFP-ADE2*	Bystricky et al., 2004
GA-2194	GA-180	*ade2-1::HIS3p-GFP-lacI-URA3p-tetR-GFP-ADE2, SIR3::URA3::* Δ*sir3::HIS3, TELIII-R::lacO-TRP1 (RS::E-HMR-I-TRP1-lacO::RS)*	MRG206-1 from M. Gartenberg (Robert Wood Johnson Medical School, Piscataway, NJ)
GA-2193	GA-2254	*TELIII-L::tetO-LEU2*	This study
GA-2198	GA-1320	*TELV-R::lacO-TRP1*	This study
GA-2197	GA-1320	*TELV-L::lacO-TRP1*	This study
GA-1459	GA-1320	*TELVI-R::lacO-lexAop-TRP1*	Heun et al., 2001b
GA-2200	GA-1320	*TELVI-L::lacO-TRP1*	This study
GA-2817	GA-2200	*ku70::KanMX*	This study
GA-2465	GA-1320	*TELXIV-R::lacO-TRP1*	This study
GA-1985	GA-1320	*TELXIV-L::lacO-TRP1*	Hediger et al., 2002
GA-1461	GA-1320	*ARS607::lacO-TRP1*	Heun et al., 2001b
GA-2196	GA-1320	*MAT***a** *(194 kb)::lacO-TRP1*	This study
GA-2195	GA2194**a** x GA2193α	*MAT***a** *ade2-1::HIS3p-GFP-lacI-URA3p-tetR-GFP-ADE2, his3-11,-15 ura3-1, TELIII-L::tetO-LEU2, TELIII-R::lacO-TRP1*	Bystricky et al., 2004
GA-2255	GA-180	*ade2-1::HIS3p-CFP-lacI-URA3p-tetR-YFP-ADE2*	Bystricky et al., 2004
GA-2337	GA-2255	*TELIII-L::tetO-LEU2, TELIII-R::lacO-TRP1*	This study
GA-2199	GA-180	*TELV-L::tetO-LEU2, TELV-R::lacO-TRP1 ura3-1::HIS3p-CFP-lacI-URA3 ade2-1:: URA3p-tetR-YFP-ADE2*	Bystricky et al., 2004
GA-2201	GA-2255	*TELVI-L::tetO-LEU2, TELVI-R::lacO-TRP1*	Bystricky et al., 2004
GA-2202	GA-2255	*TELVI-L::tetO-LEU2, TELXIV-L::lacO-TRP1*	Bystricky et al., 2004
GA-2805	GA-2201	*yku70::HIS3*	This study
GA-2806	GA-2201	*sir4::NAT1*	This study
GA-2468	GA-2255	*TELXIV-L::tetO-LEU2, TELXIV-R::lacO-TRP1*	This study
GA-2757	S288C	*TELV-L::tetO-LEU2, TELXIV-R::lacO-TRP1 ade2::HISp-CFP-LacI-URAp-TR-YFP-ADE ade2del1 his3d0el200 leu2del0 met15del0 trp1del63 ura3del0*	This study
GA-2252	GA-180	*his3-11,-15::HIS3p-YFP-lacI-HIS3, SPC42::SPC42-CFP-URA3, TELVI-R::lacO-TRP1 + pGHV45 (Nop1-CFP, CEN, ADE2)*	This study
GA-2253	GA-2198	*SPC42::SPC42-CF-URA3 + pGHV45 (Nop1-CFP, CEN, ADE2)*	This study

at the *ade2*-1 locus. Where indicated GFP-Nup49 fusions were integrated as described previously (Heun et al., 2001a). Complete *yku70* and *sir4* deletions were obtained using a PCR-based gene deletion technique (Longtine et al., 1998; Hediger et al., 2002). pBM197 contains a Spc42-CFP fusion for integration at the *URA3* gene (a gift from M. Peter, Eidgenössische Technische Hochschule Zürich, Zürich, Switzerland). Strains used are listed in Table III.

Microscopy

For live imaging, cultures grown in YPD to 0.2–0.4 × 10^7 cells/ml were imaged on SC agar + 4% glucose patches or in a Ludin chamber at 30°C. Initially, attempts to visualize Tel 3L and 3R using CFP-lacI/YFP-tetR failed, thus Tel 3L and 3R were visualized with GFP fusions differentiated by spot size (GA-2195) and later with CFP/YFP (GA-2337). Telomere–telomere distance measurements were compared and found to be identical in both strains. Subnuclear position assignment was performed on 19-image (170-nm step size) stacks of living cells acquired on a microscope (model IX70; Olympus) as described previously (Heun et al., 2001b; Hediger et al., 2002). IF and time-lapse imaging were performed on the Zeiss LSM510 with a 100x Plan-Apochromat objective (NA = 1.4), and images were acquired in multi-tracking mode using lines at 633, 488, and 543 nm and 10–25% power. 3D stacks on fixed cells were typically 16 slices of 0.2 μm or 10 of 0.25 μm, whereas live imaging was performed in single tracking mode with closed pinhole (1–1.2 airy units; GFP at 488 nm with 0.1–1.0% transmission; CFP-YFP at 458 nm and 514 nm, with 1–25% transmission) on seven sections of 0.4 μm. The maximum speeds for 2D acquisition were 80 ms per image (four averages/ROI 30 × 30) and 1.10s for 3D images (7 sections/4 averages/ROI 30 × 30). After quantification, data were routinely Gauss-filtered to reduce noise for presentation. Chromatic aberration is corrected before image-capture by alignment of 0.1 and 0.2 μm Tetraspeck Microsphere signals (Molecular Probes). FRAP of nuclear rim was performed using 50 iterations of 100% power pulses of the 488-nm laser.

Quantitative analyses of distance, position and dynamics

Distances were measured using the Zeiss LSM510 Confocal software version 2.5. Y/CFP and IF signals were scored on 3D stacks using 40–160 nuclei per point, monitoring nuclear integrity through nucleolar shape and nuclear diameter. Tagged telomere position percentages in zone 1 were compared with a random distribution by *t* test (Hediger et al., 2002), with a 95% confidence interval. 2D time-lapse series of GFP or YFP-CFP spots were analyzed with MetaMorph Offline v. 4.6r6 (Universal Imaging). For each strain 8–12 videos from two to three independent cultures were combined and averaged. MSD analysis was performed as described previously (Heun et al., 2001b; Vazquez et al., 2001) with modifications as detailed in Results.

The IMARIS software (Bitplane) was used to determine coordinates of the center of the fluorescent spots imaged in 3D over time. Reliable coordinates in 3D could be obtained from 4 out of 12 videos taken for each strain. Videos in 2D were also analyzed. Representations of the trajectories projected onto the three imaged planes were obtained using Mathematica. Direction cosines were determined for every vector, which joins two neighboring points of the trajectories of two separate fluorescent spots (frames analyzed for 3D videos were as follows: $n = 162$ for wt, $n = 178$ for *yku70*, $n = 70$ for *sir4*). Similar analysis was performed on 2D videos for which the numbers of frames were as follows: $n = 1099$ for wt, $n = 1053$ for *yku70*, $n = 829$ for *sir4*, $n = 971$ for Tel6L-14L. The mean of correlations (Pearson's correlation coefficient, c) in each (x, y, z) direction (or x, y in the 2D videos) was determined. This value (c) expresses the degree of linear relationship between two variables and is equal to the average cross product of the variables in standardized form. Pearson's c values can range between −1.00 and +1.00, with the latter signifying a perfect positive relationship, whereas −1.00 shows a perfect negative relationship. The smallest correlation is zero.

Online supplemental material

Fig. S1 shows chromosomes 3, 5, and 6 loop back on themselves. Fig. S2 shows the position of telomeres relative to the NE. Fig. S3 shows 2D distances between the telomeres during time-lapse imaging. Videos 1–6. Online supplemental material is available at http://www.jcb.org/cgi/content/full/jcb.200409091/DC1.

We thank J. Dorn and F. Neumann for MSD data, F. Hediger for telomere localization data, A. Taddei, F. Hediger, and F. Neumann for critical reading of the manuscript, and M. Peter and M. Gartenberg for plasmids and strains. We also thank the members of the Gasser lab for stimulating discussions and advice.

Our research is supported by the Swiss National Science Foundation and "Frontiers in Genetics" NCCR program.

Submitted: 20 September 2004
Accepted: 16 December 2004

References

Aragon-Alcaide, L., and A.V. Strunnikov. 2000. Functional dissection of in vivo interchromosome association in *Saccharomyces cerevisiae*. *Nat. Cell Biol.* 2:812–818.

Belgareh, N., and V. Doye. 1997. Dynamics of nuclear pore distribution in nucleoporin mutant yeast cells. *J. Cell Biol.* 136:747–759.

Belmont, A.S. 2001. Visualizing chromosome dynamics with GFP. *Trends Cell Biol.* 11:250–257.

Berg, H. 1993. Random Walks in Biology. Princeton University Press, Princeton, NJ. 164 pp.

Bradnam, K.R., C. Seoighe, P.M. Sharp, and K.H. Wolfe. 1999. G+C content variation along and among *Saccharomyces cerevisiae* chromosomes. *Mol. Biol. Evol.* 16:666–675.

Bystricky, K., P. Heun, L. Gehlen, J. Langowski, and S.M. Gasser. 2004. Long-range compaction and flexibility of interphase chromatin in budding yeast analysed by high resolution imaging techniques. *Proc. Natl. Acad. Sci. USA.* 101:16495–16500.

Cremer, M., J. von Hase, T. Volm, A. Brero, G. Kreth, J. Walter, C. Fischer, I. Solovei, C. Cremer, and T. Cremer. 2001. Non-random radial higher-order chromatin arrangements in nuclei of diploid human cells. *Chromosome Res.* 9:541–567.

Cremer, M., K. Kupper, B. Wagler, L. Wizelman, J. von Hase, Y. Weiland, L. Kreja, J. Diebold, M.R. Speicher, and T. Cremer. 2003. Inheritance of gene density-related higher order chromatin arrangements in normal and tumor cell nuclei. *J. Cell Biol.* 162:809–820.

Cooper, J.P., Y. Watanabe, and P. Nurse. 1998. Fission yeast Taz1 protein is required for meiotic telomere clustering and recombination. *Nature.* 392:828–831.

Croft, J.A., J.M. Bridger, S. Boyle, P. Perry, P. Teague, and W.A. Bickmore. 1999. Differences in the localization and morphology of chromosomes in the human nucleus. *J. Cell Biol.* 145:1119–1131.

Dekker, J., K. Rippe, M. Dekker, and N. Kleckner. 2002. Capturing chromosome conformation. *Science.* 295:1306–1311.

Dundr, M., and T. Misteli. 2001. Functional architecture in the cell nucleus. *Biochem. J.* 356:297–310.

Fransz, P., J.H. De Jong, M. Lysak, M.R. Castiglione, and I. Schubert. 2002. Interphase chromosomes in *Arabidopsis* are organized as well defined chromocenters from which euchromatin loops emanate. *Proc. Natl. Acad. Sci. USA.* 99:14584–14589.

Funabiki, H., I. Hagan, S. Uzawa, and M. Yanagida. 1993. Cell cycle-dependent specific positioning and clustering of centromeres and telomeres in fission yeast. *J. Cell Biol.* 121:961–976.

Gartenberg, M.R., F.R. Neumann, T. Laroche, M. Blaszczyk, and S.M. Gasser. 2004. Sir-mediated repression can occur independently of chromosomal and subnuclear contexts. *Cell.* 119:955–967.

Gasser, S.M., and M.M. Cockell. 2001. The molecular biology of the SIR proteins. *Gene.* 279:1–16.

Gotta, M., T. Laroche, A. Formenton, L. Maillet, H. Scherthan, and S.M. Gasser. 1996. The clustering of telomeres and colocalization with Rap1, Sir3, and Sir4 proteins in wild-type *Saccharomyces cerevisiae*. *J. Cell Biol.* 134:1349–1363.

Guacci, V., E. Hogan, and D. Koshland. 1997. Centromere position in budding yeast: evidence for anaphase A. *Mol. Biol. Cell.* 8:957–972.

Hall, I.M., K. Noma, and S.I. Grewal. 2003. RNA interference machinery regulates chromosome dynamics during mitosis and meiosis in fission yeast. *Proc. Natl. Acad. Sci. USA.* 100:193–198.

Hediger, F., F.R. Neumann, G. Van Houwe, K. Dubrana, and S.M. Gasser. 2002. Live imaging of telomeres: yKu and Sir proteins define redundant telomere-anchoring pathways in yeast. *Curr. Biol.* 12:2076–2089.

Hediger, F., A. Taddei, F.R. Neumann, and S.M. Gasser. 2004. Methods for visualizing chromatin dynamics in living yeast. *Methods Enzymol.* 375:345–365.

Heun, P., T. Laroche, M.K. Raghuraman, and S.M. Gasser. 2001a. The positioning and dynamics of origins of replication in the budding yeast nucleus. *J. Cell Biol.* 152:385–400.

Heun, P., T. Laroche, K. Shimada, P. Furrer, and S.M. Gasser. 2001b. Chromosome dynamics in the yeast interphase nucleus. *Science.* 294:2181–2186.

Hochstrasser, M., D. Mathog, Y. Gruenbaum, H. Saumweber, and J.W. Sedat. 1986. Spatial organization of chromosomes in the salivary gland nuclei of *Drosophila melanogaster*. *J. Cell Biol.* 102:112–123.

Jin, Q., E. Trelles-Sticken, H. Scherthan, and J. Loidl. 1998. Yeast nuclei display prominent centromere clustering that is reduced in nondividing cells and in meiotic prophase. *J. Cell Biol.* 141:21–29.

Kanoh, J., and F. Ishikawa. 2001. spRap1 and spRif1, recruited to telomeres by Taz1, are essential for telomere function in fission yeast. *Curr. Biol.* 11:1624–1630.

Kleckner, N., and B.M. Weiner. 1993. Potential advantages of unstable interactions for pairing of chromosomes in meiotic, somatic, and premeiotic cells. *Cold Spring Harb. Symp. Quant. Biol.* 58:553–565.

Longtine, M.S., A. McKenzie III, D.J. Demarini, N.G. Shah, A. Wach, A. Brachat, P. Philippsen, and J.R. Pringle. 1998. Additional modules for versatile and economical PCR-based gene deletion and modification in *Saccharomyces cerevisiae*. *Yeast.* 14:953–961.

Marshall, W.F., A. Dernburg, B. Harmon, D.A. Agard, and J.W. Sedat. 1996. Specific interactions of chromatin with the nuclear envelope: positional determination within the nucleus in *Drosophila melanogaster*. *Mol. Biol. Cell.* 7:825–842.

Marshall, W.F., A. Straight, J.F. Marko, J. Swedlow, A. Dernburg, A. Belmont, A.W. Murray, D.A. Agard, and J.W. Sedat. 1997. Interphase chromosomes undergo constrained diffusional motion in living cells. *Curr. Biol.* 7:930–939.

Ostashevsky, J. 2002. A polymer model for large-scale chromatin organization in lower eukaryotes. *Mol. Biol. Cell.* 13:2157–2169.

Parada, L.A., P.G. McQueen, and T. Misteli. 2004. Tissue-specific spatial organization of genomes. *Genome Biol.* 5:R44.

Partridge, J.F., K.S. Scott, A.J. Bannister, T. Kouzarides, and R.C. Allshire. 2002. cis-acting DNA from fission yeast centromeres mediates histone H3 methylation and recruitment of silencing factors and cohesin to an ectopic site. *Curr. Biol.* 12:1652–1660.

Peters, A.H., D. O'Carroll, H. Scherthan, K. Mechtler, S. Sauer, C. Schofer, K. Weipoltshammer, M. Pagani, M. Lachner, A. Kohlmaier, et al. 2001. Loss of the Suv39h histone methyltransferases impairs mammalian heterochromatin and genome stability. *Cell.* 107:323–337.

Pryde, F.E., and E.J. Louis. 1999. Limitations of silencing at native yeast telomeres. *EMBO J.* 18:2538–2550.

Rabl, C. 1885. über Zellteilung. *Morphol. Jahrbuch.* 10:214–330.

Raghuraman, M.K., E.A. Winzeler, D. Collingwood, S. Hunt, L. Wodicka, A. Conway, D.J. Lockhart, R.W. Davis, B.J. Brewer, and W.L. Fangman. 2001. Replication dynamics of the yeast genome. *Science*. 294:115–121.

Ryan, R.F., D.C. Schultz, K. Ayyanathan, P.B. Singh, J.R. Friedman, W.J. Fredericks, and F.J. Rauscher III. 1999. KAP-1 corepressor protein interacts and colocalizes with heterochromatic and euchromatic HP1 proteins: a potential role for Kruppel-associated box-zinc finger proteins in heterochromatin-mediated gene silencing. *Mol. Cell. Biol.* 19:4366–4378.

Scherf, A., L.M. Figueiredo, and L.H. Freitas-Junior. 2001. Plasmodium telomeres: a pathogen's perspective. *Curr. Opin. Microbiol.* 4:409–414.

Scherthan, H. 2001. A bouquet makes ends meet. *Nat. Rev. Mol. Cell Biol.* 2:621–627.

Shaw, P.J., R. Abranches, A. Paula Santos, A.F. Beven, E. Stoger, E. Wegel, and P. Gonzalez-Melendi. 2002. The architecture of interphase chromosomes and nucleolar transcription sites in plants. *J. Struct. Biol.* 140:31–38.

Spector, D.L. 2003. The dynamics of chromosome organization and gene regulation. *Annu. Rev. Biochem.* 72:573–608.

Taddei, A., F. Hediger, F.R. Neumann, C. Bauer, and S.M. Gasser. 2004. Separation of silencing from perinuclear anchoring functions in yeast Ku80, Sir4 and Esc1 proteins. *EMBO. J.* 23:1301–1312.

Trelles-Sticken, E., M.E. Dresser, and H. Scherthan. 2000. Meiotic telomere protein Ndj1p is required for meiosis-specific telomere distribution, bouquet formation and efficient homologue pairing. *J. Cell Biol.* 151:95–106.

Vazquez, J., A.S. Belmont, and J.W. Sedat. 2001. Multiple regimes of constrained chromosome motion are regulated in the interphase *Drosophila* nucleus. *Curr. Biol.* 11:1227–1239.

Yang, C.H., E.J. Lambie, J. Hardin, J. Craft, and M. Snyder. 1989. Higher order structure is present in the yeast nucleus: autoantibody probes demonstrate that the nucleolus lies opposite the spindle pole body. *Chromosoma.* 98:123–128.